Quasi-Equilibrium AFM Measurement of Disjoining Pressure in Lubricant Nano-Films I: Fomblin Z03 on Silica

ARTICLE *in* LANGMUIR · JANUARY 2007

Impact Factor: 4.46 · DOI: 10.1021/la0612522 · Source: PubMed

5 AUTHORS, INCLUDING:

Yiao Hsia
Western Digital Corporation
75 PUBLICATIONS **1,245** CITATIONS
SEE PROFILE

Paul M. Jones
Seagate Technology
62 PUBLICATIONS **968** CITATIONS
SEE PROFILE

Quasi-Equilibrium AFM Measurement of Disjoining Pressure in Lubricant Nano-Films I: Fomblin Z03 on Silica

Adam P. Bowles,† Yiao-Tee Hsia,‡ Paul M. Jones,‡ James W. Schneider,† and Lee R. White*,†

Department of Chemical Engineering, Carnegie Mellon University, Pittsburgh, Pennsylvania 15213-3890, and Seagate Research Center, Seagate Technology, 1251 Waterfront Place, Pittsburgh, Pennsylvania 15222-4215

Received May 4, 2006. In Final Form: August 10, 2006

We have identified conditions in which the atomic force microscope can be used to stretch a meniscus of a perfluoropolyether (PFPE) lubricant pinned between an AFM tip and a nanometer-thick PFPE film to obtain the disjoining pressure of the film. Under quasi-equilibrium conditions, the chemical potential of the film can be equated to that of the stretched meniscus. A theory is presented that provides a complete description of the capillary force of a stretched meniscus. Fits of the theory to quasi-equilibrium force-extension curves yield the effective meniscus curvature and, by extension, the disjoining pressure of the underlying film. AFM force curves collected at varying film thicknesses compare very well with predictions from Lifshitz theory of dispersive interactions in thin films, with no adjustable parameters. This complete description of meniscus deformation during atomic force microscopy force−extension experiments makes possible the measurement of unknown disjoining pressures as required for screening of lubricant−overcoat combinations required for next-generation data storage systems.

Introduction

Central to the understanding of foam stability and wetting is knowledge of the disjoining pressure (Π) of thin liquid films (reviewed by Bergeron[1]). The disjoining pressure is defined as the force per area exerted between the two interfaces that bound the thin liquid films, owing to a combination of molecular-level interactions. These include van der Waals, electrostatic, and structural components. Physically, the disjoining pressure can be envisioned as an internal force driving film swelling that balances external forces (such as gravity and capillarity) acting to thin the film. The disjoining pressure can be substantially altered by the addition of surfactants, with attendant impact on film thickness. The curvature of liquid bridges in contact with the thin film is also impacted as equilibrium between the film and meniscus is established.

Measurements of disjoining pressure as a function of film thickness ("disjoining pressure isotherms") can be accomplished by several different methods, each requiring a means to tune an external force. Disjoining pressures of liquid films are frequently measured using a thin-film balance.[2] This apparatus uses a porous glass annulus holding a volume of liquid. The ring is placed on the substrate in a sealed chamber where gas pressure is controlled. The chemical potential of the bulk liquid in the ring is controlled by a manometer fused to the glass ring and exposed at the open end to some reference pressure. Lowering the open end below the ring applies a negative pressure, ΔP, to the liquid, and the film in the center of the ring thins to achieve equilibrium with the bulk fluid. The thickness of the entrained film can then be measured using an interferometric technique. The chemical potential of the liquid under pressure ΔP is

$$\mu_L^{Liq}(\Delta P) = \mu_L^\circ + \upsilon_L \Delta P \quad (1)$$

where μ_L° is the chemical potential of the bulk lubricant and υ_L is the molar volume of the liquid. The chemical potential of the thin film μ_L^{Film} is[3]

$$\mu_L^{Film} = \mu_L^\circ - \upsilon_L \Pi(h) \quad (2)$$

so that equality of film and bulk liquid chemical potentials requires

$$\Pi(h) = -\Delta P \quad (3)$$

Unfortunately, this technique is limited to the measurement of small to moderate disjoining pressures due to the way in which the bulk pressure is applied. The measurement of disjoining pressure of liquid films formed by condensation from the vapor phase[4−7] is a common technique but is limited to films of volatile liquids. Another technique used to measure the disjoining pressure of thin lubricant films is a contact angle study.[8−12] In these experiments, drops of nonwetting liquids are placed on the film and their contact angles are measured. Thermodynamic con-

* To whom correspondence should be addressed. E-mail: white@andrew.cmu.edu.

† Carnegie Mellon University.

‡ Seagate Technology.

(1) Bergeron, V. *J. Phys. Condens. Matter* **1999**, *11*, R215−R238.

(2) Claesson, P. M.; Ederth, T.; Bergeron, V.; Rutland, M. W. *Adv. Colloid Interface Sci.* **1996**, *67*, 119−184.

(3) Hsia, Y. T.; Jones, P. M.; White, L. R. *Langmuir* **2004**, *20*, 10073−10079.

(4) Gee, M. L.; Healy, T. W.; White, L. R. *J. Colloid Interface Sci.* **1989**, *131*, 18−23.

(5) Gee, M. L.; Healy, T. W.; White, L. R. *J. Colloid Interface Sci.* **1989**, *133*, 514−516.

(6) Christenson, H. K. *Phys. Rev. Lett.* **1994**, *73*, 1821−1824.

(7) Crassous, J.; Charlaix, E.; Loubet, J. L. *Phys. Rev. Lett.* **1997**, *78*, 2425−2428.

(8) Tyndall, G. W.; Waltman, R. J.; Pocker, D. J. *Langmuir* **1998**, *14*, 7527−7536.

(9) Tyndall, G. W.; Leezenberg, P. B.; Waltman, R. J.; Castenada, J. *Tribol. Lett.* **1998**, *4*, 103−108.

(10) Tyndall, G. W.; Waltman, R. J. *MRS Symp. Proc.* **1998**, *517*, 403−414.

(11) Waltman, R. J.; Kurshudov, A.; Tyndall, G. W. *Tribol. Lett.* **2002**, *12*, 163−169.

(12) Waltman, R. J.; Pocker, D. J.; Tyndall, G. W. *Tribol. Lett.* **1998**, *4*, 267−275.

10.1021/la0612522 CCC: $33.50
Published on Web 11/01/2006

siderations of this technique show that certain assumptions as to the displacement of the film must be made.[3] At present, surface rearrangements in the film under the influence of the nonwetting fluid and the role of contact angle hysteresis are not well understood.

We have developed a direct method of measuring the disjoining pressure that can be applied to nonvolatile, highly viscous films such as those presented by perfluoropolyether (PFPE) lubricants of magnetic data storage systems. PFPE polymers are ubiquitous magnetic recording hard disk lubricants. They are functionally well-suited to perform both as a boundary lubricant and as a protective layer where their high chemical inertness and thermal stability are especially important.[13−15] An extensive research literature exists probing the PFPE lubricant−surface interaction;[16−18] this has been primarily focused on the effects of functional constituents and polymer chain length on surface mobility, stability and wetting behaviors.[16−21] Central to these efforts has been the measurement of macroscopic film properties, either evolving in time or perturbed by surface film coverage.[22] Using phenomenological arguments, several studies have sought to connect the measured macroscopic properties to molecular-surface attributes, which can become tenuous if indirect probes of the spread films are used.[8] Furthermore, these measurements need to be direct, repeatable, and easily obtained to be practicable when probing and sorting numerous lubricant−overcoat combinations. Novel overcoat materials need to be compatible with hard-drive lubricants which provide protection against wear that would otherwise result from collisions between the recording head and the overcoat. While proper lubricant function is best measured by directly assessing wear characteristics of lubricant−overcoat combinations, such measurements can be time-consuming and fail to provide the kind of molecular-level insight that would inform the improved formulation and design of these systems. Thus, a probe of a nanofilm should provide molecular insight into the wanted attributes of a lubricant (i.e., wetting, stability, etc.), thereby facilitating the design of the next generation of hard disk drive lubricants.

The method uses atomic force microscopy (AFM) to measure the force required to slowly stretch a meniscus of PFPE bridging a film-covered sample and a spherical probe. Fitting the resulting force vs probe−sample separation data (force curves) to theoretical capillary force curves allows the disjoining pressure to be calculated. This technique was pioneered by Mate and co-workers who first demonstrated that AFM could be used to probe lubricant properties (including measurement of disjoining pressure) by stretching a lubricant meniscus.[20,23−26] The present work differs from these original studies in the use of full theoretical capillary force curves which permit the measurement of $\Pi(h)$ for thicker films, a thorough understanding of the choice of AFM parameters (i.e., probe radius and cantilever spring constant) required to measure a given film, and a detailed experimental analysis of the dynamics for the establishment of the equilibrium conditions required by the method.

Collection of disjoining-pressure isotherms ($\Pi(h)$) for lubricant−overcoat combinations is critical to assessing their performance. An ideal hard-disk lubricant wets the overcoat on the disk, quickly flows to heal defects in surface coverage, and has a low vapor pressure. Each of these characteristics can be related to the disjoining pressure, $\Pi(h)$, of the lubricant film, defined as[3]

$$\Pi(h) \equiv -\frac{\partial E_{\mathrm{SLA}}}{\partial h} \tag{4}$$

where h is the lubricant film thickness and $E_{\mathrm{SLA}}(h)$ is the interaction energy per unit area between the (multilayered) substrate, S, and the air halfspace, A, across the lubricant, L. The interaction energy $E_{\mathrm{SLA}}(h)$ contains contributions from van der Waals, polar, hydrogen-bonding, and steric or structural forces in the general case.

Restoration of the film after a depletion event will occur if the disjoining pressure is positive:[3]

$$\Pi(h) > 0 \tag{5}$$

and for the spread film to be stable, we require[3]

$$\frac{\partial \Pi(h)}{\partial h} < 0 \tag{6}$$

If the disjoining pressure is positive but eq 6 is not satisfied, the film will minimize its total free energy by forming a bimodal height distribution. The formation of such structures, which have been observed experimentally,[22] is expected to be problematic in practical data storage systems. As such, the disjoining pressure of lubricant films provides a useful measure of the wettability of the lubricant on substrata, and its thickness dependence is a measure of the ability of the film to resist and heal defects. More thorough discussions of the role of disjoining pressure in wetting and the factors involved in film stability are considered elsewhere.[3,27−29]

In dynamic spreading, the film thickness, $h(x,t)$, at position x on the substrate at time t is given by[23,30]

$$\frac{\partial h}{\partial t} = \frac{\partial}{\partial x}\left(D(h)\frac{\partial h}{\partial x}\right) \quad D(h) = -\frac{h^3}{3\eta}\frac{\partial \Pi(h)}{\partial h} \tag{7}$$

where η is the Newtonian viscosity of the lubricant. For simple lubricants obeying eqs 5 and 6, the effective diffusion coefficient, $D(h)$, for the film height is positive and restoring flows after a head crash follow the usual diffusive course. However, for the typical disk-surface lubricant Zdol (PFPE oligomers with terminal hydroxyl groups), the disjoining pressure does not satisfy eq 6 for all film thicknesses (i.e., it is not monotonically decreasing with increasing film thickness) and the effective diffusion

(13) Li, L.; Jones, P. M.; Hsia, Y. T. *Tribol. Lett.* **2004**, *16*, 21−27.
(14) Li, L.; Jones, P. M.; Merzlikine, A. G.; Hsia, Y. T. *Tribol. Lett.* **2004**, *17*, 953−959.
(15) Jones, P. M.; Li, L.; Hsia, Y. T. In *STLE/ASME International Joint Tribology Conference*; American Society of Mechanical Engineers: Ponte Vedra Beach, FL, 2003; pp 9−15.
(16) Kasai, P. H.; Raman, V. *Tribol. Lett.* **2003**, *15*, 15−28.
(17) Kasai, P. H.; Raman, V. *Tribol. Lett.* **2004**, *16*, 29−36.
(18) Lei, R. Z.; Gellman, A. J.; Jones, P. *Tribol. Lett.* **2001**, *11*, 1−5.
(19) Ma, X.; Gui, J.; Marchon, B.; Jhon, M. S.; Bauer, C. L.; Rauch, G. C. *IEEE Trans. Magn.* **1999**, *35*, 2454−2456.
(20) Mate, C. M.; Novotny, V. J. *J. Chem. Phys.* **1991**, *94*, 8420−8427.
(21) Waltman, R. J.; Kobayashi, N.; Shirai, K.; Khurshudov, A. *Tribol. Lett.* **2004**, *16*, 151−162.
(22) Hyun, K. I.; Mate, C. M.; Hannibal, K. A.; Perry, S. S. *Phys. Rev. Lett.* **1999**, *82*, 3496−3499.
(23) Mate, C. M. *J. Appl. Phys.* **1992**, *72*, 3084−3090.
(24) Mate, C. M. *Phys. Rev. Lett.* **1992**, *68*, 3323−3326.
(25) Mate, C. M.; Lorenz, M. R.; Novotny, V. J. *J. Chem. Phys.* **1989**, *90*, 7550−7555.
(26) Blackman, G. S.; Mate, C. M.; Philpott, M. R. *Phys. Rev. Lett.* **1990**, *65*, 2270−2273.
(27) Derjaguin, B. V. *Theory of Stability of Colloids and Thin Films*; Plenum: New York, 1989.
(28) Starov, V. M. *Adv. Colloid Interface Sci.* **1992**, *39*, 147−173.
(29) Sharma, A. *Langmuir* **1993**, *9*, 3580−3586.
(30) Jhon, M. S.; Phillips, D. M.; Vinay, S. J.; Messer, C. T. *IEEE Trans. Magn.* **1999**, *35*, 2334−2337.

coefficient becomes negative over a range of film thicknesses. Restoring flows in the thickness region of negative $D(h)$ exhibit stepped film profiles which do not present the usual flow behavior.[19,30] Such films will continue to exhibit the bimodal thickness distribution discussed above. These permanently "scarred" surfaces will affect the performance of the recording head at low fly heights and may leave some parts of the disk surface permanently less protected. Recent studies have shown the presence of lubricant "moguls" within the region flown by the recording head.[31] These features are moundlike areas of periodic circumferential lubricant that are due to the interaction of the dynamical pressurization of the flying head and the lubricant on the surface. The typical hard-disk lubricant experiences terraced flow behavior when the lubricant is mounded in this manner. This thickness distribution may evolve, leaving areas of the media unprotected by the lubricant and further impacting the dynamical spacing between the flying read−write transducer and the media surface.

The primary goal of the present study is to establish that quasi-equilibrium measurements of the meniscus stretching force can be used to ascertain the disjoining pressure. Use of Fomblin Z03, which is believed to interact with the substrate almost exclusively by van der Waals interactions, provides a useful proof-of-concept for the AFM method. In the next three sections, we present the theory underpinning the technique, the theoretical capillary force analysis, and the restrictions placed on the measurement by the nature of the AFM measurement itself. In subsequent sections, we present an experimental study of the technique where we examine the role of wetting period and stage retraction speed on the minimization of nonequilibrium effects and the measured disjoining pressure of the $Z/SiO_2/Si$ system. These results are compared to the theoretical predictions of Lifshitz theory for the van der Waals component of the disjoining pressure and the earlier experimental results of Mate and Novotny[20] and Fukuzawa et al.[32,33]

Equilibrium AFM Pull-off Force Measurement

The AFM pull-off force measurement can be used to extract the disjoining pressure of a lubricant film as outlined below. Contact of the probe with the film-bearing substrate produces a meniscus of bulk lubricant which comes to equilibrium with the film in time. The chemical potential of the lubricant in the meniscus is given by eq 2 where ΔP is now the Laplace pressure of the meniscus:[25]

$$\Delta P = \gamma_{LA}\left(\frac{1}{r_1} + \frac{1}{r_2}\right) \tag{8}$$

Here r_1 and r_2 are the local negative in-plane and positive axial radii of curvature, respectively (see Figure 1), and γ_{LA} is the interfacial tension of the lubricant−air surface. If the lubricant in the meniscus is in thermodynamic equilibrium with that on the surface:

$$\Pi(h) = -\Delta P = \frac{\gamma_{LA}}{r_{eff}} \tag{9}$$

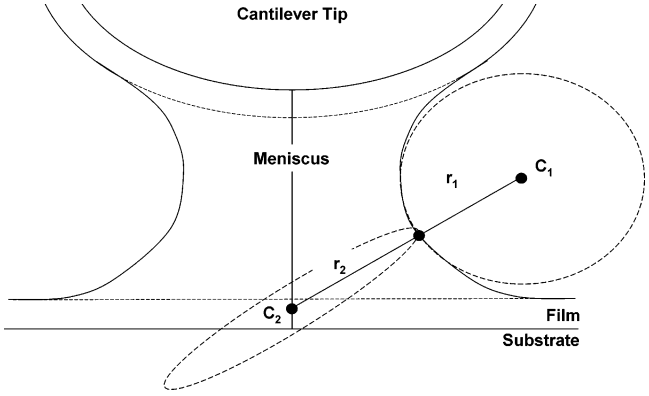

Figure 1. Definition of principal radii of curvature (r_1 and r_2) for a saddle-shaped meniscus.

where the (positive) effective radius of curvature, r_{eff}, is defined by

$$\frac{1}{r_{eff}} = -\left(\frac{1}{r_1} + \frac{1}{r_2}\right) \tag{10}$$

Given that the volume of film lubricant is large compared to the meniscus volume, the film far from the contact point is unchanged and its disjoining pressure is determined by the film thickness. Equilibrium between the film and the meniscus during pull-off requires that r_{eff} must remain constant. Mate et al.[25] derived the pull-off force, $F(D)$, as

$$F(D) = -4\pi\gamma_{LA}R\left[1 - \frac{D-h}{2r_{eff}} + \cdots\right] \tag{11}$$

where D is the probe−substrate separation distance obtained from the AFM measurement assuming that r_{eff} and D are small. Thus Mate's method simply requires the measurement of $F(D)$ as a function of D and the extraction of r_{eff} via eq 11 from the slope. Equation 9 then yields the disjoining pressure for that film thickness. As we shall show below, eq 11 is not an accurate expression for the capillary force under a range of experimental conditions and that care must be exercised to ensure that equilibrium is maintained between film and meniscus during the pull-off experiment.

Theoretical Capillary Force Calculation

In this section we present the calculation of the theoretical capillary force that the meniscus in equilibrium exerts on the spherical probe particle attached to the AFM cantilever. Equation 10, with r_{eff} a given constant, is a differential equation for the meniscus shape when it is in equilibrium with the lubricant film during pull-off. In Appendix 1, we solve eq 10 to obtain the separation distance, D, as

$$D = h + h_p + r_{eff}\left[\Delta(\alpha,\theta_p) - \frac{1}{\lambda}(1 + \cos\theta_p)\right] \tag{12}$$

where the function $\Delta(\alpha,\theta)$ is defined in eq A.6, the angle θ_p is defined in eq A.9 and

$$\alpha = \frac{r_{eff}}{r_0} \quad \lambda = \frac{r_{eff}}{R} \tag{13}$$

Here r_0 is the radius at which the meniscus contacts the film (see

(31) Ma, X.; Tang, H.; Stirniman, M.; Gui, J. *IEEE Trans. Magn.* **2002**, *38*, 112−117.
(32) Fukuzawa, K.; Kawamura, J.; Deguchi, T.; Zhang, H.; Mitsuya, Y. *IEEE Trans. Magn.* **2004**, *40*, 3183−3185.
(33) Fukuzawa, K.; Kawamura, J.; Deguchi, T.; Zhang, H.; Mitsuya, Y. *J. Chem. Phys.* **2004**, *121*, 4358−4363.

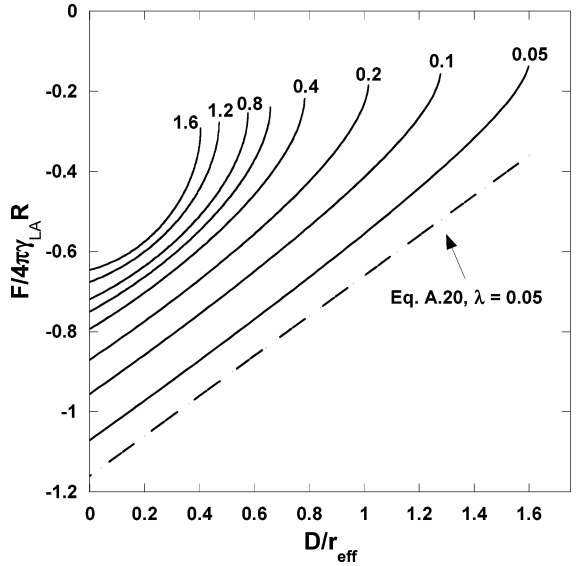

Figure 2. Scaled capillary force, F^* (eq 15), versus scaled tip displacement for various values of $\lambda = r_{eff}/R$. The dashed line is the approximate result given by eq A.20 for $\lambda = 0.05$($h = h_p = 4$ nm, $R = 0.5$ μm).

Figure 12). The pull-off force, $F(D)$, measured by the AFM deflection is given by

$$F(D) = \pi r_0^2 \Delta P \tag{14}$$

so that we may write, from eq 9

$$F(D) = (4\pi\gamma_{LA}R)F^* \quad F^* = -\frac{\lambda}{4\alpha^2} \tag{15}$$

In Figure 2 we plot the scaled pull-off force, F^*, as a function of D/r_{eff} for various values of λ. We note (eq 12) that this curve is strictly a function of the parameter $(h + h_P)/R$ in addition to λ, but for all cases of interest, this parameter is very small and the resultant curve is quite insensitive to its value. In the plot, we have taken $h = h_P = 4$ nm and probe radius $R = 0.5$ μm. We show only the physically accessible part of the $F(D)$ curve in Figure 2. The segment of the capillary force curve with negative slope is unstable, and the spring instability of the AFM system would lead to breakage of the meniscus and a jump apart before this portion of the pull-off curve is reached. In the stable region, the form of the theoretical equilibrium $F(D)$ curve is characteristically upward curving, and this is a useful indicator of whether the experimental pull-off measurement is an equilibrium one. Note that the maximum separation for a stable equilibrium meniscus is of order r_{eff}, and this observation serves to limit the range of r_{eff} values tested in the curve fitting of experimental pull-off data. In Figure 2, we show Mate's linear result as a dashed line for the case of $\lambda = 0.05$ where the approximations entailed in eq 11 are valid. At larger λ values, both the slope and contact ($D = 0$) value of the capillary force differ significantly from the predictions of eq 11.

To emphasize this point, in Figure 3 we plot $F^*(0)$, the scaled contact capillary force, as a function of scaled meniscus radius, λ (again with $h = h_P = 4$ nm and probe radius $R = 0.5$ μm). The deviation from Mate's small r_{eff} result ($F^* \approx 1$) as r_{eff} increases is evident. In Figure 4, we plot the scaled initial slope $(\lambda/2\pi\gamma_{LA})$-$(\partial F/\partial D)|_{D=0}$ as a function of scaled meniscus radius, λ (with $h = h_P = 4$ nm and probe radius $R = 0.5$ μm). As λ increases, the initial slope becomes significantly smaller than unity—the small r_{eff} value for the scaled initial slope given by eq 11. Thus, the

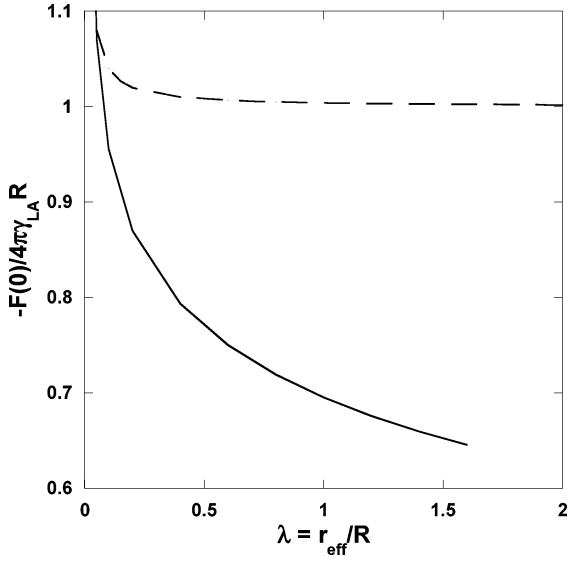

Figure 3. Scaled contact capillary force $F(0)/(4\pi\gamma_{LA}R)$ versus scaled meniscus curvature $\lambda = r_{eff}/R$ ($h = h_p = 4$ nm, $R = 0.5$ μm). The approximate result from eq A.20 is the dashed line.

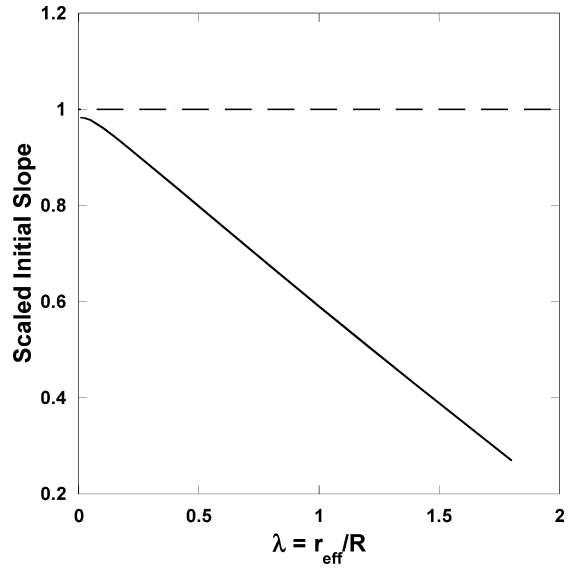

Figure 4. Scaled initial slope of the capillary force curve $(\lambda/2\pi\gamma_{LA})$-$(\partial F/\partial D)|_{D=0}$ versus scaled meniscus curvature $\lambda = r_{eff}/R$ ($h = h_p =$ 4 nm, $R = 0.5$ μm). The approximate result from eq A.20 is the dashed line.

use of eq 11 in the analysis of experimental pull-off curves will overestimate the value of r_{eff} and lead to underestimation of the corresponding disjoining pressure when r_{eff} is large.

Implications for the AFM Experiment

The capillary force theory developed above has several implications for the actual AFM pull-off experiment which we address below. Figure 5 is an idealized AFM pull-off force curve that captures the phenomena we see in our data. The region from A to B represents contact between tip and the sample substrate upon retraction of the stage. Contact persists not only while the cantilever is relaxing to its rest state but past this point due to attractive van der Waals interactions between the substrate and the tip and the capillary forces from the lubricant meniscus. At a very small separation, the probe−substrate adhesion peaks and the total force begins to decrease. At B, the slope of the force curve becomes equal to the cantilever spring constant, K, and these forces become insufficient to hold the cantilever on the

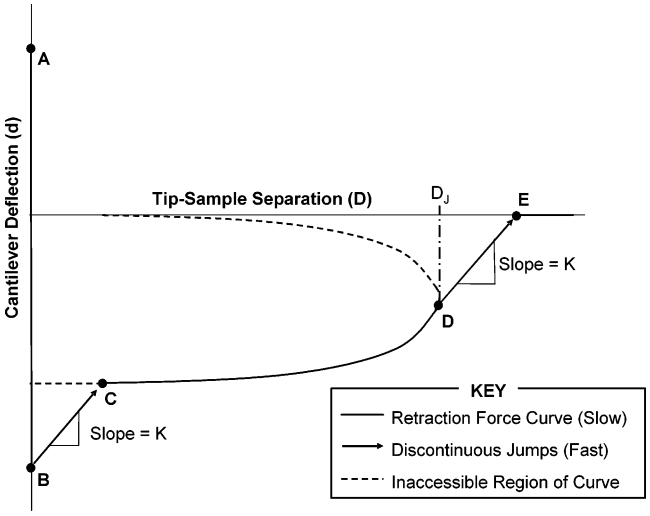

Figure 5. Schematic of a retraction AFM-derived force curve collected on a stretched fluid meniscus between the AFM tip and a surface. Points A−B indicate contact between tip and surface, B−C is separation of the surfaces with a trapped liquid bridge spanning them, C−D is the meniscus stretching, and D−E is the jump reflecting breakage of the liquid bridge.

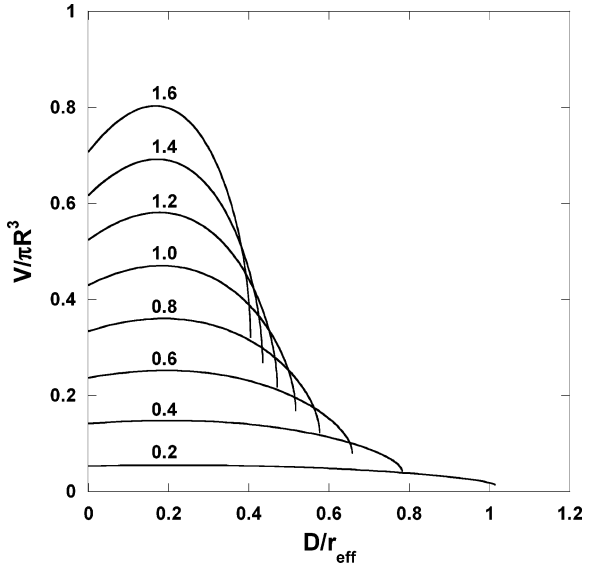

Figure 6. Scaled meniscus volume $V/\pi R^3$ (eq A.23) versus scaled separation for various values of scaled meniscus curvature $\lambda = r_{eff}/R$ ($h = h_p = 4$ nm, $R = 0.5$ μm).

surface and the cantilever jumps out of contact. If the spring constant is too small, this jump-out can bypass the entire meniscus curve, especially when r_{eff} is small (large Π), and the capillary force curve has a large initial slope. For sufficiently large K values, the system will jump out to a point C on the capillary force curve. Since the equilibrium capillary force plot curves upward, a necessary condition to experimentally observe the capillary curve is

$$K > \left.\frac{\partial F}{\partial D}\right|_{D=0} \tag{16}$$

The theoretical capillary force calculation for a given r_{eff} can therefore indicate the spring constant required to observe it by AFM. As a rule of thumb, the larger the disjoining pressure is (i.e., the thinner the lubricant film), the stiffer the cantilever must be to measure it.

To the right of C, the meniscus stretches on stage retraction until point D (separation distance D_J) where the slope of the capillary curve again equals K. Here, a second mechanical instability occurs and the cantilever quickly relaxes to E following a path of slope K and the meniscus breaks. To the right of E, the cantilever has no external forces acting upon it. If the pull-off force is measured sufficiently slowly that the meniscus remains in thermodynamic equilibrium with the substrate film, then λ is a constant and α increases as D increases (see eq 13). Thus, from eqs 12 and 15, we may write the instability condition as

$$\alpha^4 \frac{\partial}{\partial \alpha^2}\left[\Delta(\alpha,\theta_p) - \frac{1}{\lambda}(1+\cos\theta_p)\right]_{D_J} = \frac{\pi\gamma_{LA}}{K_C} \tag{17}$$

The derivative is evaluated by a simple numerical integration, as shown in Appendix 1. Equations 12, 15, and 17 serve to completely specify the theoretical $F(D)$ curve from $D = 0$ to $D = D_J$ for given values of r_{eff} and probe radius R.

As probe−substrate separation is increased, the volume of lubricant within the meniscus (at constant r_{eff}) changes. To maintain equilibrium, lubricant must be pumped to or from the surrounding substrate film and the dynamics of this process is controlled by the diffusion coefficient (see eq 7) and hence, by the disjoining pressure in the region around the edge of the meniscus. In Appendix 1, we have calculated the excess meniscus volume, V (eq A.23), and in Figure 6, we plot $V/\pi R^3$ for various λ values as a function of the scaled separation distance, D/r_{eff} (with $h = h_P = 4$ nm and probe radius $R = 0.5$ μm). Note that the excess meniscus volume in our experimental system ($\sim\pi R^3$) is at least 5 orders of magnitude smaller than the total volume of lubricant on the surface ($V = hA$ where $A \sim 1$ cm^2 is the surface area of the AFM sample). This validates our original assumption that the film far from the meniscus is unperturbed. We note that, for small separations, D, the excess volume in the equilibrium meniscus increases slightly as the surfaces separate. However, for separations approaching the jump-out point, it decreases markedly. To maintain equilibrium here, a considerable volume of liquid must flow back into the surrounding film. When retraction is faster than this excess fluid can be pumped away, the meniscus is capable of stretching to larger separation distances than permitted under equilibrium conditions before the instability occurs. It is likely, at these separations, that the experimental pull-off measurement is nonequilibrium and therefore unreliable. Accordingly, in curve fitting the experimental capillary force curves, the data near jump-out is given small weight. The excess volume change on separation becomes more pronounced for larger r_{eff} values (i.e., thicker films), and these systems will be more likely to exhibit anomalous, nonequilibrium pull-off force curves.

Finally we note that, for a given radius of the probe sphere, there is a maximum value of r_{eff} that can be measured with that sphere, viz. when r_{eff} is such that the meniscus contacts the probe sphere at $r_p = R + h_p$ where $\theta_p = \pi/2$ at zero separation of sphere and substrate. For larger r_{eff} values, the meniscus will flood the cantilever. From (eq A.9) we see that the α value corresponding to this maximum r_{eff} value is

$$\alpha = \frac{\lambda^{max}}{[1+2\lambda^{max}]^{1/2}} \tag{18}$$

and from eq 12 with $D = 0$

$$\lambda^{max}\Delta\left(\frac{\lambda^{max}}{[1+2\lambda^{max}]^{1/2}}, \pi/2\right) = 1 - \frac{h+h_p}{R} \tag{19}$$

Table 1. Ellipsometry-Derived Film Thicknesses for Fomblin Z03 Films Dip-Coated onto Silica Substrates

film thickness (nm)	concentration (g PFPE/L solution)	dipping speed (mm/min)
1.2	2.00	50
2.5	2.00	100
3.1	4.01	45
3.9	5.05	60

Table 2. Meniscus Curvature and Disjoining Pressure Obtained from Fits of AFM Force Curves on Fomblin Z03 Films of Varying Thickness[a]

film thickness (nm)	retraction velocity (nm/s)	r_{eff} (nm)	disjoining pressure (Pa)
1.2	0.0547	12.5 ± 2.5	1.680×10^6
2.5	0.1	185 ± 10	1.135×10^5
3.1	0.1	495 ± 15	4.242×10^4
3.9	0.0547	790 ± 20	2.658×10^4

[a] The error for each r_{eff} is associated with the fitting. Disjoining pressure was calculated using the equilibrium condition between Laplace pressure and disjoining pressure.

Solving this equation for λ^{max}, we obtain

$$\frac{r_{eff}^{max}}{R} = \lambda^{max} \simeq 2.53 \qquad (20)$$

where we have neglected the weak dependence on the $(h + h_P)/R$ parameter. For a given probe radius, the AFM pull-off experiment is restricted to films where $r_{eff} \leq r_{eff}^{max}$.

Materials and Methods

Dip-Coating. The glassware used in the dip-coating process was soaked in chromate cleaning solution (Fisher Scientific, Pittsburgh PA) for 15 min followed by copious rinsing with deionized water. Prior to dip-coating, undoped silicon wafers (International Wafer Service) were cleaned for 20 min using a UV−ozone cleaner (Jelight Company, Inc.). Dip coating was accomplished using the dipping apparatus of a Langmuir−Blodgett film balance (KSV 5000, KSV Instruments). Dips were performed at the retraction velocities listed in Table 2. The immersion time was about 1 min, although this parameter is not expected to impact the final layer thickness.[34] Following constant-speed retraction, wafers were broken in half: one-half was used in ellipsometry measurements of film thickness, and a portion of the other half was probed using the AFM technique. Two parameters were varied to control film thickness: concentration of Fomblin Z03 in solution and retraction velocity of the wafer. Lubricant layer thicknesses (1−4 nm) obtained under various dip-coating conditions are shown in Table 1. Imaging of the dip-coated films by dynamic AFM and imaging ellipsometry revealed no vacancies of the type reported by Fukuzawa et al.[33] for Z03 on silica. As they report, this is likely due to our UV−ozone cleaning of the wafers prior to film deposition.

Ellipsometry. Lubricant layer thicknesses were confirmed by ellipsometry using a custom-built rotating-analyzer ellipsometer.[35,36] Because only half of a wafer was dip-coated, the thickness of both the transparent layers—lubricant and native oxide—could be measured. Three measurements were taken at a random location on the uncoated silica region and averaged to yield the native oxide layer thickness at that point. Additional locations (three to five) in the bare oxide region were examined. At each location, three measurements were taken. These measurements gave an estimate of the variation in silica thickness on the wafer. Deviations were less than 1 nm from the mean silica thickness. The same procedure was repeated on the film-covered region. Typically, the Fomblin Z03 film thickness deviated about 0.3 nm from the mean depending upon location.

Table 3. Disjoining Pressure and Hamaker Function for the System Silicon/Silica/ZO3/Air) Obtained from Retarded Lifshitz Calculation (see Appendix 2) with a Silica Layer Thickness of 2.0 nm and Varying Z03 Thicknesses

film thickness (nm)	disjoining pressure (Pa)	Hamaker function (J)
0.1	9.14×10^8	-1.73×10^{-20}
0.5	7.42×10^6	-1.84×10^{-20}
1.0	9.76×10^5	-2.05×10^{-20}
1.5	3.10×10^5	-2.25×10^{-20}
2.0	1.40×10^5	-2.42×10^{-20}
2.5	7.64×10^4	-2.56×10^{-20}
3.0	4.67×10^4	-2.67×10^{-20}
3.5	3.08×10^4	-2.75×10^{-20}
4.0	2.15×10^4	-2.82×10^{-20}
4.5	1.56×10^4	-2.87×10^{-20}
5.0	1.17×10^4	-2.90×10^{-20}

AFM Experiments. AFM force−displacement curves were collected using a commercial system (Multimode, Nanoscope IIIa controller, Veeco Metrology) with a closed-loop piezo scanner (PicoForce, Veeco Metrology). Cantilevers (Novascan) used had a rectangular, diving-board geometry with a nominal spring constant of 14 N/m, and were coated with a 30 nm layer of gold to reduce optical interference. A 0.5 ± 0.125 μm radius spherical silica tip was attached to the end of the cantilever by the manufacturer. Before these cantilevers were mounted in the AFM, they were rinsed with Vertrel XF and UV−ozone cleaned for 20 min to remove any residual PFPE from previous experimental runs. The AFM was enclosed in a hood with small trays of $CaSO_4$ (Drierite) to maintain a relative humidity of 15−25% within the hood. The AFM was also surrounded by foam insulation to minimize temperature fluctuations. To minimize thermal drifts, which can be significant given the very slow retract speeds utilized, the cantilever was illuminated by the AFM laser overnight to achieve a steady temperature. After these initial preparations, several force curves were performed in a day using the methodology described below. In the case of the 1.2, 2.5, and 3.1 nm films, the tip was left in contact with the sample substrate for 30 min to allow sufficient time for PFPE to wet the sphere to equilibrium. At this point, a retraction force curve was collected until full separation was achieved. A variety of retraction speeds ranging from 0.0547 nm/s to 1.0 nm/s were tested for each sample. The technique employed for the 3.9 nm film was identical to that for the other films with the exception that the waiting period prior to force curve acquisition for the 3.9 nm film sample was increased to 3 h. This was to allow more time for the larger-volume meniscus to form.

Results and Discussion

Appropriate Conditions for AFM Force Measurements. Two key experimental parameters to be studied were the retraction speed and the waiting time required to obtain quasi-equilibrium measurements. The effect of retraction speed is shown in Figure 7, where the length of the stretched liquid bridge progressively increases as the retraction speed is increased from 0.1 to 1.0 nm/s. We expect that faster retraction velocity corresponds to a meniscus that is further removed from the equilibrium condition. At faster speeds, the meniscus has a larger volume because of insufficient drainage and this allowed one to stretch the meniscus to larger tip−sample separations than would be expected for a constant r_{eff} curve. Superior fits were obtained between the experimental data and Lifshitz theory at slow retraction velocities (0.0547−0.1 nm/s), and these rates were used for the data described in the next section.

The effect of the in-contact waiting time prior to retraction is shown in Figure 8, where the stretched meniscus length increases on increasing the waiting time from 30 min to 3 h. It is reasonable to presume that the waiting time is required to allow lubricant

(34) Gao, C.; Lee, Y. C.; Chao, J.; Russak, M. *IEEE Trans. Magn.* **1995**, *31*, 2982−2984.
(35) Azzam, R. M. A.; Bashara, N. M. *Ellipsometry and Polarized Light*, 3rd ed.; Elsevier Science: New York, 1989.
(36) Muller, R. H. *Adv. Electrochem. Electrochem. Eng.* **1973**, *9*, 167−226.

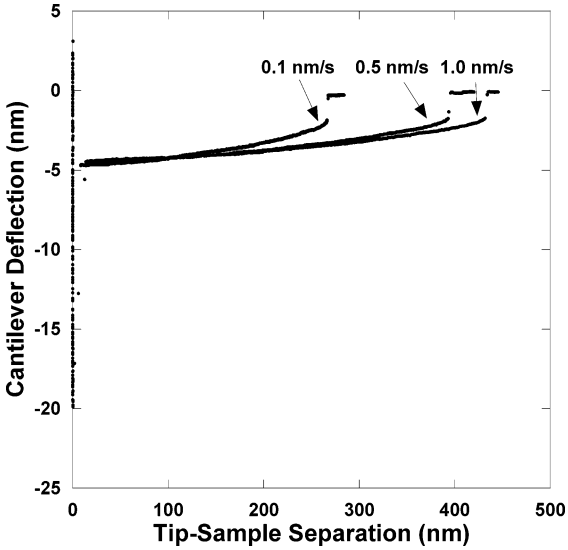

Figure 7. AFM experiments performed on a 3.1 nm thick Fomblin Z03 film at different retraction speeds.

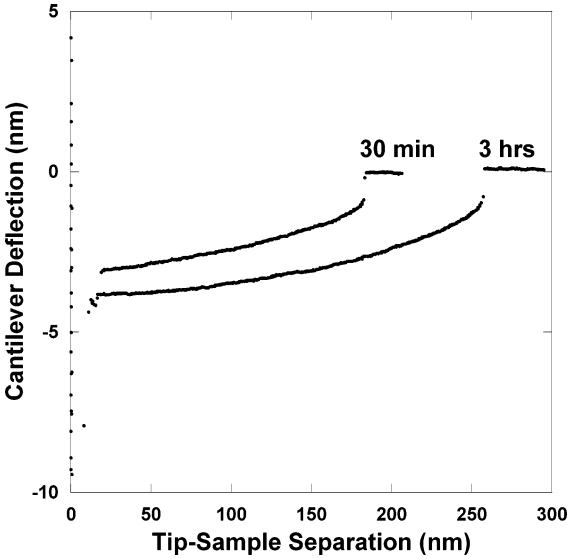

Figure 8. Effect of different wetting periods on the shape of AFM force curves (3.9 nm thick film). Wetting times are shown above the data. For both curves, the retraction velocity was 0.5 nm/s.

to spread onto the AFM tip, filling the meniscus to the equilibrium volume. We have also observed that, when using AFM tips that have not been cleaned following the previous experiment, much shorter waiting times were required to yield force curves similar to the 3 h result of Figure 8. This indicates that the lubricant remains held to the sphere after the meniscus is broken and can be used in subsequent force curves.

Selecting the correct cantilever probe size was also important to obtain useful data. Initial trials were conducted using a 2.5 μm radius spherical particle as the probe but tip wetting became prohibitively time-consuming because of the increased meniscus volume the larger tip engenders. Figure 6 supports these observations. Calculations suggest that a 2.5 μm particle draws an order of magnitude more lubricant than a 0.5 μm one, since the meniscus volume scales as tip radius cubed. However, as discussed above, the smaller the probe, the lower the upper limit on the thickness of film that can be examined. As film thickness increases, the volume of the equilibrium meniscus increases until it engulfs the tip. When tip flooding occurs, the meniscus exerts very large forces on the cantilever that are not modeled by the theoretical capillary force model described earlier.

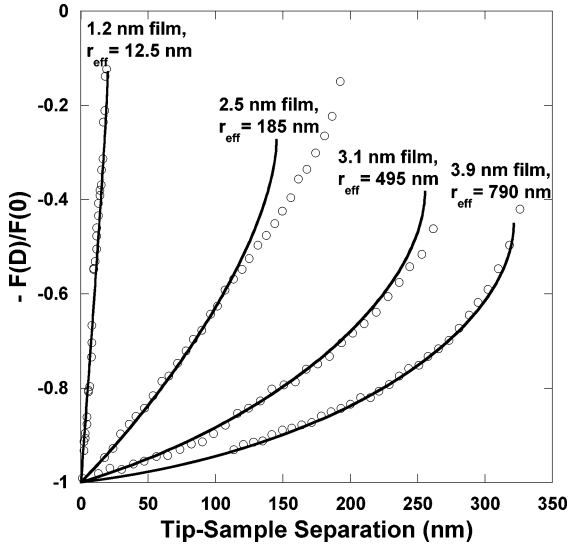

Figure 9. Normalized pull-off force curves $F(D)/F(0)$ for the four films in Table 1. The experimental contact force, $F(0)$, is obtained by extrapolation of the accessible small separation data. For ease of viewing, only every 30th point of the experimental data (circles) is plotted. The solid curves are the best-fit theoretical force curves.

Data Fitting. To obtain accurate fits, we scaled the experimental force curve, $F(D)$, with respect to the contact value, $F(0)$, obtained by extrapolating the experimental capillary force curve to zero separation. This scaling helped to ameliorate uncertainties in cantilever spring constants (~20%), as well as significant variation in cantilever tip diameter (~25%). Figure 9 shows four representative curves, along with fits to eqs 12−15, demonstrating a very good agreement, with a small deviation near meniscus breakage. This is likely due to the failure to completely pump the excess meniscus volume back into the film at larger separations, obviating the quasi-equilibrium assumption as discussed above. The experimentally observed jump-out distance, D_J, is always a little larger than the theoretical prediction as expected if the excess meniscus volume has not been pumped away.

The output of the data fitting of Figure 9 is the effective meniscus radius, r_{eff}. This quantity gives the disjoining pressure directly through eq 9. These results are given in Figure 10. Calculation of the disjoining pressure from Lifshitz theory (Appendix 2) shows very good agreement with the experimentally derived values for disjoining pressure. It should be emphasized that the Lifshitz calculations use no adjustable parameters; the dispersive properties of the various components of the film were obtained from published spectroscopic data. In the case of the 1.2 nm film, the theory curve does pass within the error bars but may exhibit a small positive departure from Lifshitz theory. This may have a physical rationale. A 1.2 nm thick Fomblin Z03 film is approximately a monolayer. At such film thickness, it is possible that the surface influences the PFPE molecules and encourages structure atypical of their random bulk conformation, and this may explain any positive deviation from purely van der Waals behavior. On the other hand, the deviation may have its origin in the neglected small correction factor in the capillary force calculation (discussed in Appendix 1) which accounts for the influence of disjoining pressure on the microscopic meniscus profile. We have not investigated these possibilities further in the present study.

We also display in Figure 10 some earlier disjoining pressure results extracted from the graphical data of Mate and Novotny[20] for a Fomblin Z of molecular weight 5000 (roughly comparable to that of the Z03 lubricant presented in this work) on silica. At

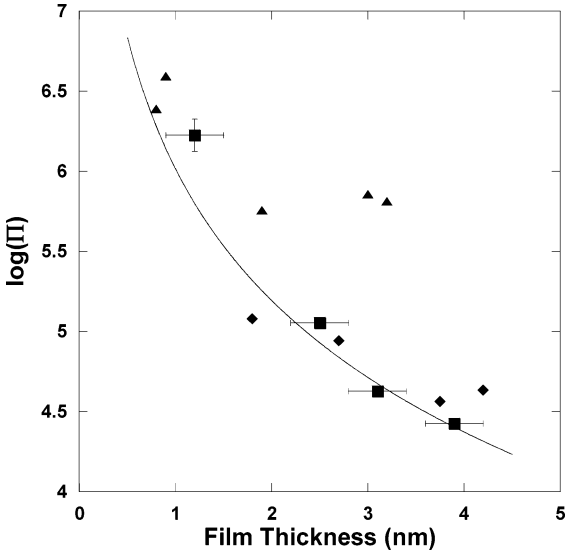

Figure 10. Disjoining pressure of Z03 on Si/SiO_2 versus film thickness. Squares are values obtained from fitting AFM force data of Figure 9, and the line is derived from Lifshitz theory (Appendix 2). Triangles are from Mate and Novotny,[20] and diamonds are from Fukuzawa et al.[33]

small film thicknesses, there is good agreement between our results, the earlier study, and the van der Waals theoretical prediction. However, at larger thicknesses, the earlier data are considerably larger (an order of magnitude at a thickness of 3 nm) than both the theoretical prediction and the results of the present work. We believe that this is due to the failure, in the previous studies, to allow sufficient wetting time to establish an equilibrium meniscus at the larger film thicknesses. Thus, pull-off forces were obtained with smaller effective radii of curvature than equilibrium resulting in larger disjoining pressures being reported. We have observed identical behavior in our present study when the wetting period is not sufficiently prolonged.

Recently, Fukuzawa et al. have provided a new method to obtain disjoining pressure isotherms by applying thin liquid films to substrates with microfabricated grooves and imaging the resulting meniscus using dynamic-mode AFM.[32,33] The method is similar in spirit to the one presented here, in that equilibrium is established between a curved meniscus and a thin film and the film disjoining pressure ascertained from the shape of the meniscus. In order for assumptions in their analysis to hold, the method is limited to film thicknesses above about 3 nm. However, their method can be applied to thicker films that would engulf the AFM probe used in the method described here, and the two methods should be viewed as complementary. Comparing data they collected over the range of 3−5 nm (for Fomblin Z03 on silica of molecular weight 4000), we find excellent agreement (Figure 10). Taken together, the data of Figure 10 suggest that the method presented here gives excellent agreement with both Lifshitz theory and established experimental methods in the range of 1−4 nm.

In Figure 11, we have plotted the theoretical diffusion coefficient, which governs the dynamics of film flow in Z03 lubricant nanofilms using the van der Waals disjoining pressure shown in Figure 10 and the definition eq 7. A comparison with our experimental data was obtained by first fitting the disjoining pressure isotherm to a power-law function (a and b are fitting parameters):

$$\Pi = ah^b \qquad (21)$$

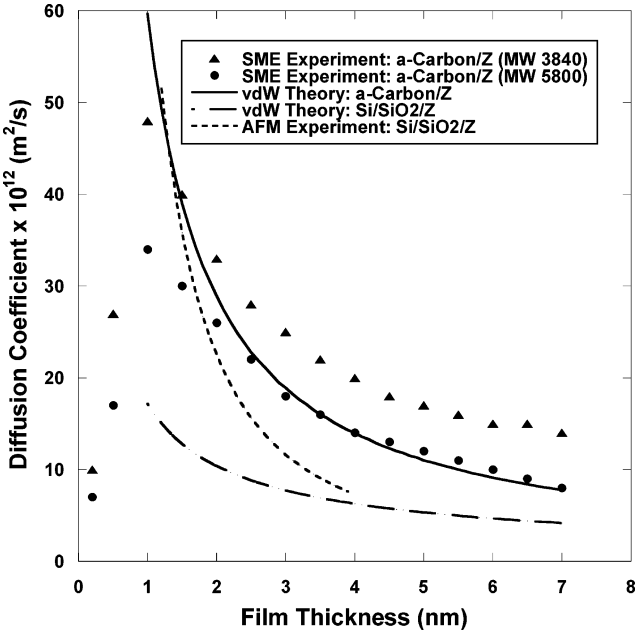

Figure 11. Diffusion coefficient for Fomblin Z on various substrates. The triangles and circles are taken from the scanning microellipsometry (SME) studies of Kim et al.[37] of Z on amorphous carbon for two molecular weights which span the molecular weight of the Z03 used in the present AFM study. The diffusion coefficients calculated from the theoretical van der Waals disjoining pressure of Z03 on amorphous carbon (continuous curve) and on Si/SiO_2 (large dashed curve) are displayed as a function of film thickness. The results of the present AFM study for Si/SiO_2/ZO3 are also shown (small dashed curve). Calculated diffusion coefficients are obtained by differentiating disjoining pressure data via eq 7.

The thickness derivative of eq 21 was inserted into eq 7 to derive the diffusion coefficient (Figure 11). It differs somewhat from the theoretical van der Waals diffusion coefficient and may reflect the contribution of structural forces at small thickness; however, it should be noted that only a small number of data points have been collected in this regime. For an additional comparison, we also plot in Figure 11 diffusion coefficient data taken from the study of Kim et al.[37] of the spreading of Z films on amorphous carbon surfaces by scanning microellipsometry (SME). The results for two molecular weights of Z are shown. These span the molecular weights of the Z in our AFM study. These SME data are larger than the experimental and theoretical diffusion coefficients for the Si/SiO_2/Z system. This is due mainly to the difference in van der Waals force between the carbon and the silicon substrates, as can be clearly seen from the plot of the theoretical diffusion coefficient calculated from eq 7 using the van der Waals disjoining pressure for Z on amorphous carbon. In fact, there is a remarkable agreement between the SME experiments for the higher MW Fomblin and the theoretical van der Waals curve, which would seem to indicate that the assumption of bulk Newtonian viscous behavior in these thin films is well approximated.

The diffusion coefficient can be seen to be a decreasing function of film thickness of magnitude $\sim 10^{-11}$ m^2/s for Z films on these substrates. Since a meniscus of excess volume $\sim \pi R^3$ must be drawn from the surface film over a radial extent $\sim \sqrt{R^3/h}$, the time scale for the meniscus pumping process is $R^3/D(h)h \approx 10^2$ s. The wetting time required to create the equilibrium meniscus from the film is significantly larger than this time scale because

(37) Kim, M. C.; Phillips, D. M.; Ma, X.; Jhon, M. S. *J. Colloid Interface Sci.* **2000**, *228*, 405−409.

the disjoining pressure contribution to the lubricant flux acts against the Laplace pressure gradient in the inward flowing situation.

Conclusions

We have identified conditions in which AFM force measurements of the stretching of a liquid bridge formed between a PFPE lubricant film and an AFM tip yield the disjoining pressure of the film, a critical parameter when judging its wear-reducing properties in hard-disk applications. Judicious selection of the AFM tip size, spring constant, retraction speed, and in-contact waiting time are needed to establish the requisite quasi-equilibrium condition that equates the film chemical potential with that of the stretched meniscus. Fits of the AFM force curve to the internal Laplace pressure of a stretched meniscus give the disjoining pressure. Such data collected on films of Fomblin Z03, which are believed to interact purely by van der Waals forces, give excellent agreement with theoretical predictions of disjoining pressure based on Lifshitz theory, which considers only van der Waals interactions. For more sophisticated lubricants such as Zdol, preliminary AFM studies on silicon and nitrogenated silicon surfaces[38] show large structural/polar contributions to the total disjoining pressure which is a strong function of the chemical composition of the substrate. With an appreciation of the constraints on the AFM measurement, the present technique offers a straightforward technique for assessing the role of terminating entities on the lubricant molecules, their interaction with chemical moieties on the overcoat and the dielectric properties of the overcoat in determining the dynamic response of the lubricant on disk substrates. Future work will focus on applying the method to films of industrial importance, where nondispersive interactions are crucial and require quantification.

Appendix 1. Capillary Force Calculation

Laplace's equation (eq 10) for the meniscus shape is

$$\frac{\mathrm{d}\sin\theta}{\mathrm{d}r} + \frac{\sin\theta}{r} = -\frac{1}{r_{\mathrm{eff}}} \tag{A.1}$$

where the first term on the left is the inverse of the in-plane radius of curvature (<0) and the second is the inverse of the axial radius of curvature (>0). The right-hand side is the Laplace pressure difference, Δp, in the meniscus divided by γ_{LA}, the liquid−air surface tension (eq 9). The effective radius of curvature, r_{eff}, is a constant if the meniscus remains in equilibrium with the nanofilm during pull-off. It should be appreciated that the macroscopic Laplace equation should strictly be modified when the liquid−air interface is sufficiently close to the substrate that the interaction energy, E_{SLA}, makes a significant contribution to the free energy of a surface area element.[39,40] The inclusion of the disjoining pressure term in eq A.1 makes an $\vartheta(h/r_{\mathrm{eff}})$ correction to the macroscopic result reported below.[40] As such, this microscopic profile effect can be neglected for all but the very thinnest of lubricant films where r_{eff} becomes comparable to the film thickness. For the smallest film thickness in the present study, $h/r_{\mathrm{eff}} \approx 0.1$.

(38) Jones, P. M.; Luo, M.; White, L. R.; Schneider, J.; Wu, M.-L.; Platt, C.; Li, L.; Hsia, Y.-T. *Tribol. Int.* **2005**, *38*, 528−532.
(39) White, L. R. *J. Chem. Soc., Faraday Trans. 1* **1977**, *73*, 390−398.
(40) Solomentsev, Y.; White, L. R. *J. Colloid Interface Sci.* **1999**, *218*, 122−136.

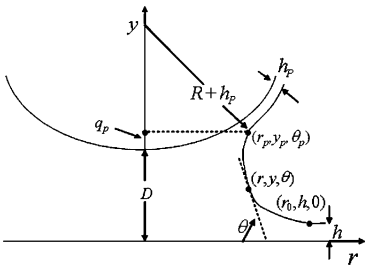

Figure 12. Geometry of the meniscus trapped between AFM tip (top) and the substrate (bottom). Variables are referred to in Appendix 1.

The geometry and coordinates are defined in Figure 12. Equation A.1 is integrated to yield

$$r\sin\theta = \frac{r_0^2 - r^2}{2r_{\mathrm{eff}}} \tag{A.2}$$

where r_0 is the radial distance at which the meniscus merges with the substrate film (see Figure 12) where $\theta = 0$. Alternatively, since $\mathrm{d}y/\mathrm{d}r = -\tan\theta$, eq A.1 can be written as

$$\frac{\mathrm{d}\cos\theta}{\mathrm{d}y} + \frac{\sin\theta}{r} = -\frac{1}{r_{\mathrm{eff}}} \tag{A.3}$$

and rearranged to yield

$$\frac{\mathrm{d}y}{\mathrm{d}\theta} = \frac{r_{\mathrm{eff}}}{1 + r_{\mathrm{eff}}\sin\theta/r} \tag{A.4}$$

Upon integration, using eq A.2 and the boundary condition $y(0) = h$, we obtain

$$y(\theta) = h + r_{\mathrm{eff}}\Delta(\alpha,\theta) \tag{A.5}$$

where

$$\Delta(\alpha,\theta) = \int_0^\theta \frac{\mathrm{d}\theta\sin\theta}{(\alpha^2\sin^2\theta + 1)^{1/2}[(\alpha^2\sin^2\theta + 1)^{1/2} + \alpha\sin\theta]} \tag{A.6}$$

and

$$\alpha = \frac{r_{\mathrm{eff}}}{r_0} \tag{A.7}$$

The meniscus contacts the spherical probe surface (radius $R + h_{\mathrm{p}}$) at (r_{p}, y_{p}, θ_{p}) where

$$\sin\theta_{\mathrm{p}} = r_{\mathrm{p}}/(R + h_{\mathrm{p}}) \tag{A.8}$$

where we assume that a film of liquid of thickness h_{P} exists on the probe surface at equilibrium. If the substrate and probe are the same material, we can expect $h = h_{\mathrm{P}}$, but otherwise, h_{P} is another parameter of the system, albeit a rather insensitive one. Using eq A.2 we have, from eq A.8

$$\theta_{\mathrm{p}} = \pi - \arcsin\left[\frac{(\lambda/\alpha)}{(1 + 2\lambda)^{1/2}}\right] \tag{A.9}$$

for contact on the bottom half of the probe (θ_p obtuse) where

$$\lambda = \frac{r_{\mathrm{eff}}}{R + h_{\mathrm{p}}} \simeq \frac{r_{\mathrm{eff}}}{R} \tag{A.10}$$

The vertical distance, q_p, from y_p to the lowest point on the probe (see Figure 12) is given by

$$r_p^2 + (q_p - R)^2 = (R + h_p)^2 \quad \text{(A.11)}$$

and the separation distance, D, between probe and substrate is

$$D = y_p - q_p \quad \text{(A.12)}$$

From eq A.5 and eq A.11 we have

$$D = h + h_p + r_{eff}\left[\Delta(\alpha,\theta_p) - \frac{1}{\lambda}(1 + \cos\theta_p)\right] \quad \text{(A.13)}$$

From eq A.2, we have

$$2\pi r\gamma_{LA}\sin\theta - \pi r^2\Delta p = -\pi r_0^2\Delta p \quad \text{(A.14)}$$

which is just the statement that, at equilibrium, the total normal force on any horizontal cross-section is a constant equal to the Laplace pressure over the area of the meniscus on the substrate. This is equal to the force on the probe (the pull-off force, F) where

$$F = \pi r_0^2\Delta p = -\frac{\pi\gamma_{LA}r_{eff}}{\alpha^2} = (4\pi\gamma_{LA}R)F^* \quad \text{(A.15)}$$

where the scaled pull-off force, F^*, is

$$F^* = -\frac{\lambda}{4\alpha^2} \quad \text{(A.16)}$$

For r_{eff}, R given, eq A.10 defines λ ($R \gg h_P$) and a specification of F^* determines α from eq A.16. Equation A.13 then defines the separation D corresponding to the scaled pull-off force F^*. In this way, the calculation of $F(D)$ for given r_{eff}, R is reduced to a straightforward numerical integration.

For small λ values, we have $1 \gg \alpha \gg \lambda$ and, from eq A.9

$$\theta_p = \pi - \frac{\lambda}{\alpha} + \ldots \quad \text{(A.17)}$$

From eq A.6, we have in this limit

$$\Delta(\alpha,\theta_p) = 2 + \ldots \quad \text{(A.18)}$$

so that eq A.13 becomes

$$D - h - h_p = r_{eff}\left[2 - \frac{\lambda}{2\alpha^2} + \ldots\right] \quad \text{(A.19)}$$

Using eq A.16, we rearrange eq A.19 to obtain

$$F(D) = -4\pi\gamma_{LA}R\left(1 - \frac{D - h - h_p}{2r_{eff}} + \ldots\right) \quad \text{(A.20)}$$

which is Mate's result (eq 11) corrected for the presence of a film on the probe sphere.

The excess volume in the meniscus (the volume of the meniscus less the volume of film that would be on the substrate and probe surfaces if the meniscus was not present) is given by

$$V = \int_{y_0 = h}^{y_p} dy\pi r^2 - V_{sp}(\theta_p) \quad \text{(A.21)}$$

where

$$V_{sp}(\theta) = \frac{\pi R^3}{3}[1 + \cos\theta]^2[2 - \cos\theta] \quad \text{(A.22)}$$

is the volume of the spherical cap (radius R) which subtends an angle $2(\pi - \theta)$ at the sphere center. Using eqs A.2 and A.4, we can rearrange eq A.21 to yield

$$V = \pi R^3\left[\frac{\lambda^3}{\alpha^2}\int_0^{\theta_p}\frac{d\theta\sin\theta}{(\alpha^2\sin^2\theta + 1)^{1/2}[(\alpha^2\sin^2\theta + 1)^{1/2} + \alpha\sin\theta]^3}\right] - V_{sp}(\theta_p) \quad \text{(A.23)}$$

When the separation distance, D, is less than the sum of film thicknesses, $h + h_P$, the term $V_{sp}(\theta_p)$ must be corrected since a piece of this spherical cap lies below the height of the films and should not have been subtracted. From the geometry of this case, we can show that the angle $2(\pi - \theta_q)$ subtended by this overcounted piece of spherical cap is defined by

$$\frac{h + h_p - D}{R} = -\lambda\left[\Delta(\alpha,\theta_p) - \frac{1}{\lambda}(1 + \cos\theta_p)\right] = 1 + \cos\theta_q \quad \text{(A.24)}$$

and for $D < h + h_P$, the excess volume is then

$$V = \pi R^3\left[\frac{\lambda^3}{\alpha^2}\int_0^{\theta_p}\frac{d\theta\sin\theta}{(\alpha^2\sin^2\theta + 1)^{1/2}[(\alpha^2\sin^2\theta + 1)^{1/2} + \alpha\sin\theta]^3}\right] - V_{sp}(\theta_p) + V_{sp}(\theta_q) \quad \text{(A.25)}$$

From eq A.6, we obtain, after some algebra,

$$\alpha^4\frac{\partial}{\partial\alpha^2}\left[\Delta(\alpha,\theta_p) - \frac{1}{\lambda}(1 + \cos\theta_p)\right] = -\frac{\lambda}{2(1 + \lambda)\cos\theta_p} - \frac{\alpha^3}{2}\int_0^{\theta_p}\frac{d\theta\sin^2\theta}{(\alpha^2\sin^2\theta + 1)^{(3/2)}} \quad \text{(A.26)}$$

a quantity we require in order to evaluate the jump-out point on the $F(D)$ curve.

Appendix 2. Retarded Calculation of Disjoining Pressure of ZO3 on Si

The interaction energy of substrate 1 interacting with substrate 2 across thickness L of medium 3 is given by[41−45]

$$E_{132}(L) = -\frac{A_{132}(L)}{12\pi L^2} \quad \text{(A.27)}$$

where the Hamaker function $A_{132}(L)$ is given by

$$A_{132}(L) = -\frac{3kT}{2}\sum_{n=0}{}'^{\infty}\int_{r_n}^{\infty} dx\, x\ln\{[1 - \Delta_{31}^E\Delta_{32}^E e^{-x}][1 - \Delta_{31}^M\Delta_{32}^M e^{-x}]\} \quad \text{(A.28)}$$

(41) Dagastine, R. R.; White, L. R.; Jones, P. M.; Hsia, Y. T. *J. Appl. Phys.* **2005**, *97*, 126106/126101−126106/126103.
(42) White, L. R.; Dagastine, R. R.; Jones, P. M.; Hsia, Y. T. *J. Appl. Phys.* **2005**, *97*, 104503/104501−104503/104507.
(43) Lifshitz, E. M. *Soviet Phys.: J. Exp. Theor. Phys.* **1956**, *2*, 73−83.
(44) Hough, D. B.; White, L. R. *Adv. Colloid Interface Sci.* **1980**, *14*, 3−41.
(45) Dzyaloshinskii, I. E.; Lifshitz, E. M.; Pitaevskii, L. P. *Adv. Phys.* **1961**, *10*, 165−209.

and

$$\Delta_{ij}^{E} = \frac{\epsilon_i s_j - \epsilon_j s_i}{\epsilon_i s_j + \epsilon_j s_i} \quad \Delta_{ij}^{M} = \frac{\mu_i s_j - \mu_j s_i}{\mu_i s_j + \mu_j s_i} \tag{A.29}$$

$$s_j^2 = x^2 + r_n^2\left(\frac{\epsilon_j}{\epsilon_3} - 1\right) \quad r_n = \frac{2L\xi_n\sqrt{\epsilon_3}}{c} \tag{A.30}$$

where

$$\epsilon_j = \epsilon_j(i\xi_n) \quad \mu_j = \mu_j(i\xi_n) \tag{A.31}$$

are the dielectric permittivity and magnetic permeability of substance j evaluated at imaginary frequency, $i\xi_n$, given by

$$\xi_n = n\xi_0 \quad \xi_0 = \frac{2\pi kT}{\hbar} \tag{A.32}$$

Here c is the speed of light, k is Boltzmann's constant, T is the absolute temperature, and $\hbar$ is Planck's constant divided by 2π. Note that $\xi_0 \approx 2.5 \times 10^{14}$ rad/s at room temperature. The prime on the summation in eq A.28 indicates that the $n = 0$ term is assigned half weight. For all materials in this study $\mu_j = 1$. The construction of the dielectric response function, $\epsilon_j(i\xi)$, for each material is discussed below.

The disjoining pressure, $\Pi_{132}(L)$, defined by

$$\Pi_{132}(L) = -\frac{\partial E_{132}}{\partial L} \tag{A.33}$$

is the force per unit area that substrate 1 exerts on substrate 2 across thickness L of medium 3 is given explicitly by[45]

$$\Pi_{132}(L) = -\frac{kT}{8\pi L^3}{\sum_{n=0}^{\infty}}' \int_{r_n}^{\infty} \times \mathrm{d}x\, x^2 \left\{ \frac{\Delta_{31}^{E}\Delta_{32}^{E}\, \mathrm{e}^{-x}}{1 - \Delta_{31}^{E}\Delta_{32}^{E}\, \mathrm{e}^{-x}} + \frac{\Delta_{31}^{M}\Delta_{32}^{M}\, \mathrm{e}^{-x}}{1 - \Delta_{31}^{M}\Delta_{32}^{M}\, \mathrm{e}^{-x}} \right\} \tag{A.34}$$

These equations must be modified when the substrate is layered, as is the case for the system Silicon(1)/Silica(4)/ZO3(3)/Air(2) considered here. In eqs A.28 and A.34, Δ_{31}^{E} is replaced by[41,42]

$$\bar{\Delta}_{31}^{E} = \frac{\Delta_{34}^{E} + \Delta_{41}^{E} \exp\left(-\frac{t_4 s_4}{L}\right)}{1 + \Delta_{34}^{E}\Delta_{41}^{E} \exp\left(-\frac{t_4 s_4}{L}\right)}$$

where t_4 is the thickness of layer 4 (the surface silica layer) and s_4 is defined in eq A.30. Analogous replacement of Δ_{31}^{M} with $\bar{\Delta}_{31}^{M}$ is also made. In this calculation $\epsilon_2(i\xi) = 1$ and we use a Ninham−Parsegian construction[41,42] for the lubricant ZO3 and the silica layer.[44] The function $\epsilon_1(i\xi)$ for silicon was calculated by a Kramers−Kronig construction[44] using $\epsilon'(\omega)$,$\epsilon''(\omega)$ data for silicon.[46] The $\epsilon(i\xi)$ function for amorphous carbon was similarly constructed from the $\epsilon''(\omega)$ data of Kovarik et al.[47]

Acknowledgment. The authors gratefully acknowledge the financial support of Seagate Technology administered through the Data Storage Systems Center at Carnegie Mellon University.

LA0612522

(46) Palik, E. D. *Handbook of Optical Constants*; Academic Press: San Diego, 1992.

(47) Kovarik, P.; Bourbon, E. B.; Prince, R. H. *Phys. Rev. Lett. B* **1993**, *48*, 12123−12129.